Hepatic NF-kB-inducing Kinase (NIK) Suppresses Mouse Liver Regeneration in Acute and Chronic Liver Diseases

Yi Xiong[1§], Adriana Souza Torsoni[1,2§], Feihua Wu[1,3], Hong Shen[1], Yan Liu[1], Xiao Zhong[1], Mark J Canet[1], Yatrik M. Shah[1], M. Bishr Omary[1], Yong Liu[4], Liangyou Rui[1,5*]

[1]Department of Molecular & Integrative Physiology, [5]Department of Internal Medicine, University of Michigan Medical School, Ann Arbor, MI 48109, USA

[2]Laboratory of Metabolic Disorders, School of Applied Sciences, University of Campinas, Limeira, São Paulo, Brazil

[3]Department of Pharmacology of Chinese Materia Medica, School of Traditional Chinese Medicine, China Pharmaceutical University, Nanjing 211198, China

[4]College of Life Sciences, the Institute for Advanced Studies, Wuhan University, Wuhan 430072, China

Keywords: Liver regeneration, hepatocyte proliferation, chronic liver disease, NF-κB-inducing Kinase, IKKα, JAK2, STAT3, interleukin 6

Abbreviations: PHx: hepatectomy; HFD: high fat diet; NIK: NF-κB-inducing Kinase; JAK2: Janus kinase 2; STAT3: Signal transducer and activator of transcription 3; AAF: 2-acetylaminofluorence.

Disclosure statement: All authors have nothing to declare.

***Corresponding author**:

Liangyou Rui, Ph.D., Department of Molecular & Integrative Physiology, University of Michigan Medical School, Ann Arbor, MI 48109, USA. E-mail: ruily@umich.edu.

Footnotes: §co-first authors: Yi Xiong and Adriana Souza Torsoni.

Summary

Reparative hepatocyte replication is impaired in chronic liver disease, contributing to disease progression; however, the underlying mechanism remains elusive. Here, we identify Map3k14 (also known as NIK) and its substrate Chuk (also called IKKα) as unrecognized suppressors of hepatocyte replication. Chronic liver disease is associated with aberrant activation of hepatic NIK pathways. We found that hepatocyte-specific deletion of *Map3k14* or *Chuk* substantially accelerated mouse hepatocyte proliferation and liver regeneration following partial-hepatectomy. Hepatotoxin treatment or high fat diet feeding inhibited the ability of partial-hepatectomy to stimulate hepatocyte replication; remarkably, inactivation of hepatic NIK markedly increased reparative hepatocyte proliferation under these liver disease conditions. Mechanistically, NIK and IKKα suppressed the mitogenic JAK2/STAT3 pathway, thereby inhibiting cell cycle progression. Our data suggest that hepatic NIK and IKKα act as rheostats for liver regeneration by restraining overgrowth. Pathological activation of hepatic NIK or IKKα likely blocks hepatocyte replication, contributing to liver disease progression.

Introduction

The liver is an essential metabolic organ that experiences metabolic stress during fasting, refeeding, and overnutrition states (1). The liver is also responsible for detoxifications of endogenous and exogenous toxic substances, thus being frequently exposed to harmful insults. Dietary hepatotoxins and gut microbiota-derived toxic substances are transported to the liver through the enterohepatic circulation, further increasing risk for liver injury. To compensate for hepatocyte loss, the liver evolves a powerful regenerative ability to maintain its homeostasis (2). After 70% of partial hepatectomy (PHx), rodents are able to regain normal liver mass within a week via reparative hepatocyte replications (3). Nevertheless, hepatocyte proliferation is severely inhibited in chronic liver diseases, including nonalcoholic fatty liver disease (NAFLD), alcoholic liver disease, and chronic exposures to hepatotoxins (4-7). Impairment in hepatocyte replications considerably precipitates liver disease progression; however, the underlying mechanism responsible for defective hepatocyte replications remains poorly understood.

In response to liver injury induced by PHx, numerous growth factors and cytokines are secreted and delivered to hepatocytes where they stimulate hepatocyte proliferation by activating multiple mitogenic pathways, including the Janus kinase 2 (JAK2)/STAT3, MAPK, PI 3-kinase, and NF-kB pathways (2). In contrast, TGFβ1 and interferon-γ inhibit hepatocyte proliferation, thereby preventing liver from overgrowth (7-9). Liver regeneration is fine-tuned by a balance between positive and negative regulators. We postulated that in chronic liver disease, the negative branch might be predominant and overcome the positive branch, leading to pathological suppression of hepatocyte proliferation and liver regeneration. However, intracellular pathways conferring hepatocyte proliferation inhibition remain elusive. In search for inhibitory pathways,

we identified Map3k14, also called NF-kB-inducing kinase (NIK), and its substrate Chuck, also referred to as IkB kinase α (IKKα).

NIK is a Ser/Thr kinase known to activate the noncanonical NF-kB2 pathway (10). It phosphorylates and activates IKKα (11). IKKα in turn phosphorylates the precursor of NF-kB2 p100, resulting in generation of the p52 form of NF-kB2 (10, 11). Mature p52 is translocated into the nucleus to activate target genes. We previously reported that metabolic stress, oxidative stress, hepatotoxins, and cytokines stimulate hepatic NIK (12, 13). Importantly, hepatic NIK is aberrantly activated in both mice and humans with NAFLD or alcoholic liver disease (12, 14). Hepatocellular stress and liver inflammation, which are associated with chronic liver disease, likely activate hepatic NIK. These observations prompted us to test the hypothesis that hepatic NIK/IKKα pathways cell-autonomously inhibit hepatocyte proliferation. In this work, we characterized hepatocyte-specific NIK ($NIK^{\Delta hep}$) and IKKα ($IKK\alpha^{\Delta hep}$) knockout mice, and examined reparative hepatocyte replications using PHx models. We found that the NIK/IKKα pathway suppresses reparative hepatocyte proliferation at least in part by inhibiting the JAK2/STAT3 pathway. This work unveils unrecognized crosstalk between the NIK/IKKα and the JAK2/STAT3 pathways involved in regulating liver regeneration.

Results

Hepatocyte-specific ablation of NIK accelerates liver regeneration. To assess the role of hepatic NIK in reparative hepatocyte proliferation, we performed 70% of PHx on mice at 8 weeks of age following the established protocols (15). $NIK^{\Delta hep}$ mice were generated by crossing *Map3k14*$^{flox/flox}$ (referred to as $NIK^{f/f}$) mice with *Albumin-Cre* drivers (16). Proliferating cells were detected by immunostaining liver sections with antibody against Ki67, a cell proliferation marker (Figure 1A). Baseline hepatocyte proliferation rates were low and comparable between

$NIK^{\Delta hep}$ and $NIK^{f/f}$ mice (Figure 1B). Number of liver proliferating $Ki67^{+}$ cells markedly increased within 48 h following PHx, and $Ki67^{+}$ cells were 85% higher in $NIK^{\Delta hep}$ relative to $NIK^{f/f}$ mice (Figure 1B). In line with these observations, the number of liver BrdU-labelled proliferating cells was also substantially higher in $NIK^{\Delta hep}$ than in $NIK^{f/f}$ mice (Figure 1C). Liver cell proliferation rates declined in both $NIK^{\Delta hep}$ and $NIK^{f/f}$ mice after 48 h post-PHx, and became comparable between these two groups at 96 h post-PHx (Figure 1B).

To verify hepatocytes proliferating, we costained liver sections with anti-Ki67 and anti-HNF4α (a hepatocyte marker) antibodies, or with anti-Ki67 and anti-F4/80 (a Kupffer cell/macrophage marker) antibodies. $HNF4\alpha^{+}$ hepatocytes accounted for 96% of $Ki67^{+}$ proliferating cells in $NIK^{\Delta hep}$ mice at 48 h post-PHx (Figure 1D,F) while $F4/80^{+}$ Kupffer cells/macrophages for <4% of $Ki67^{+}$ cells (Figure 1E,F). These data indicate that hepatic NIK is an intrinsic suppressor of hepatocyte proliferation.

We also examined the effect of NIK deficiency on hepatocyte death using TUNEL assays. The number of liver $TUNEL^{+}$ apoptotic cells was slightly lower in $NIK^{\Delta hep}$ relative to $NIK^{f/f}$ mice, but the difference was not statistically significant (Figure 1G). Plasma alanine aminotransferase (ALT) activity, a liver injury index, was comparable between $NIK^{\Delta hep}$ and $NIK^{f/f}$ mice either under basal conditions or after PHx (Figure 1H). Thus, accelerated hepatocyte proliferation cannot be explained by changes in liver injury in $NIK^{\Delta hep}$ mice.

To further confirm the role of hepatic NIK in liver regeneration, we assessed liver to body weight ratios at 2 and 4 days post-PHx. Consistently, liver/body weight ratios were significantly higher in $NIK^{\Delta hep}$ than in $NIK^{f/f}$ mice at 4 days following PHx (Figure 1I). Of note, liver/body weight ratios were similar between these two groups at 2 days post-PHx. One possible

explanation is that a 2-day period may be too short for newly-generated hepatocytes to grow in size large enough to increase liver weight.

To determine whether NIK inhibits hepatocyte cell cycle progression, we measured the levels of cyclin D1, which is believed to drive hepatocyte proliferation following PHx (7). Hepatic cyclin D1 levels were undetectable in both $NIK^{\Delta hep}$ and $NIK^{f/f}$ mice under basal conditions, and were markedly increased by PHx (Figure 2A). Importantly, hepatic cyclin D1 levels were significantly higher in $NIK^{\Delta hep}$ than in $NIK^{f/f}$ mice (Figure 2A,B). Collectively, these results support the notion that hepatic NIK may act as an intrinsic rheostat for liver homeostasis by restraining liver overgrowth.

The role of NF-kB1, MAPK, and PI 3-kinase pathways in NIK-induced suppression of hepatocyte proliferation. We next sought to interrogate the molecular mechanism of the NIK action. Expression of liver NIK rapidly increased within 12 h following PHx, but declined at 3 days post-PHx (Figure 2-figure supplement 1A). Consistently, PHx also increased phosphorylation of liver IKKα/β (Figure 2-figure supplement 1B,C). Interestingly, liver IKKα expression was also increased by PHx (Figure 2-figure supplement 1C). The NF-kB1, MAPK, and PI 3-kinase pathways are known to be involved in mediating PHx-stimulated liver regeneration (7, 17, 18). Unexpectedly, phosphorylation of hepatic IkBα, p65 (the NF-kB1 pathway), Akt (pSer473) (the PI 3-kinase pathway), ERK1/2, and JNK (the MAPK pathway) was comparable between $NIK^{\Delta hep}$ and $NIK^{f/f}$ mice at 4 h post-PHx (Figure 2C). We also did not detect difference in hepatic levels of reactive oxygen species (ROS) or hepatic expression of cytokines between $NIK^{\Delta hep}$ and $NIK^{f/f}$ mice (Figure 2D,E). Therefore, NIK suppression of liver regeneration cannot be explained by the above pathways.

NIK suppresses the JAK2/STAT3 pathway. JAK2 is known to phosphorylate and activate STAT3, which is believed to drive hepatocyte proliferation (19, 20). We postulated that NIK might suppress hepatocyte proliferation by inhibiting the JAK2/STAT3 pathway. Liver extracts were prepared at 4 h post-PHx and immunoblotted with anti-phospho-JAK2 (pTyr1007/1008) or anti-phospho-STAT3 (pTyr705) antibodies. Phosphorylation of both JAK2 and STAT3 was significantly higher in $NIK^{\Delta hep}$ mice than in $NIK^{f/f}$ littermates (Figure 3A). Baseline levels of JAK2 and STAT3 phosphorylation in the resected livers were similar between $NIK^{\Delta hep}$ and $NIK^{f/f}$ mice (Figure 2-figure supplement 1D).

To confirm that NIK directly inhibits the JAK2/STAT3 pathway, we transiently coexpressed JAK2 and STAT3 with NIK in HEK293 cells. In line with our previous reports (21), overexpressed JAK2 robustly autophosphorylated as well as phosphorylated STAT3 (Figure 3B). Strikingly, overexpression of NIK dramatically decreased tyrosine phosphorylation of both JAK2 and STAT3 (Figure 3B). Consistently, NIK was coimmunoprecipitated with JAK2 (Figure 3C). These data indicate that NIK binds to JAK2 and inhibits JAK2 activity, thereby suppressing the JAK2/STAT3 pathway.

Interleukin 6 (IL6) stimulates the JAK2/STAT3 pathway, which is required for reparative hepatocyte proliferation (22, 23). These observations prompted us to test if NIK negatively regulates the IL6/JAK2/STAT3 pathway. Mouse primary hepatocytes were transduced with NIK or β-galactosidase (β-gal) adenoviral vectors, followed by IL6 stimulation. IL6 robustly stimulated phosphorylation of STAT3 in β-gal-transduced, but not NIK-transduced, hepatocytes (Figure 3D). Collectively, these results unveil unrecognized crosstalk between NIK pathways and the JAK2/STAT3 pathway.

Hepatic IKKα suppresses liver regeneration following PHx. Given that IKKα acts downstream of NIK in the noncanonical NF-kB2 pathway, we reasoned that hepatic IKKα might also suppress liver regeneration. IKKα$^{\Delta hep}$ mice were generated by crossing *Chuk*$^{flox/flox}$ (referred to as IKKα$^{f/f}$) mice with *albumin-Cre* drivers (24). We confirmed that IKKα expression was disrupted specifically in the liver but not brain, heart, kidney, skeletal muscle, and spleen in IKKα$^{\Delta hep}$ mice (Figure 4A). We performed PHx on IKKα$^{f/f}$ and IKKα$^{\Delta hep}$ male mice at 8-9 weeks of age. The number of liver proliferating Ki67^{+} cells was significantly higher in IKKα$^{\Delta hep}$ than in IKKα$^{f/f}$ littermates at both 1 and 2 days post-PHx, and became similar between these two groups after 3 days following PHx (Figure 4B). HNF4α^{+} hepatocytes accounted for the majority of proliferating cells (Figure 4C). Consistently, liver cyclin D1 levels were significantly higher in IKKα$^{\Delta hep}$ than in IKKα$^{f/f}$ mice (Figure 4D), while liver cell death was comparable between these two groups (Figure 4E). Consequently, liver to body weight ratios were significantly higher in IKKα$^{\Delta hep}$ relative to IKKα$^{f/f}$ mice at both 5 and 7 days post-PHx (Figure 4F). Notably, liver/body weight ratios were comparable between these two groups within 3 days following PHx, likely due to lack of sufficient time for hepatocytes to grow their mass as discussed before. These results indicate that deficiency of hepatocyte IKKα, like NIK, also accelerates hepatocyte proliferation and liver regeneration in response to acute liver injury.

To gain insight into the molecular mechanism of the IKKα action, we examined the JAK2/STAT3 pathway. The levels of phosphorylation of JAK2 as well as STAT3 were significantly higher in IKKα$^{\Delta hep}$ than in IKKα$^{f/f}$ mice at 4 h post-PHx (Figure 5A,B). We also compared phosphorylation time courses during days 0-7 following PHx. IKKα phosphorylation increased while JAK2 phosphorylation decreasing during days 1-5 (Figure 5-figure supplement 1A,B). This inverse relationship further supports the notion that the NIK/IKKα pathway inhibits

the JAK2/STAT3 pathway. Ablation of hepatocyte IKKα increased phosphorylation of JAK2 and STAT3 during days 1-7 following PHx (Figure 5-figure supplement 1B). To confirm that IKKα cell-autonomously inhibits the JAK2/STAT3 pathway, IKKα was transiently coexpressed with JAK2 in HEK293 cells. IKKα was coimmunoprecipitated with JAK2 (Figure 5C), and markedly decreased JAK2 autophosphorylation and the ability of JAK2 to phosphorylate STAT3 (Figure 5D).

To determine whether NIK suppresses the JAK2/STAT3 pathway via IKKα, we transduced primary hepatocytes from IKKα$^{\Delta hep}$ (IKKα-deficient) and IKKα$^{f/f}$ (wild type) mice with NIK or green fluorescent protein (GFP) adenoviral vectors, followed by IL6 stimulation. The ability of NIK to inhibit IL6-stimulated phosphorylation of STAT3 was significantly reduced in IKKα-deficient hepatocytes compared to wild type hepatocytes (Figure 5-figure supplement 1C,D). Of note, NIK overexpression still considerately attenuated STAT3 phosphorylation in IL6-stimulated hepatocytes, compared with GFP overexpression (Figure 5-figure supplement 1D). These findings suggest that hepatic NIK suppresses the JAK2/STAT3 pathway, and possibly liver regeneration, by both IKKα-dependent and IKKα-independent mechanisms.

Deficiency of hepatic NIK accelerates liver regeneration in mice with hepatotoxin-induced liver injury. Hepatic NIK is highly activated in mice and humans with chronic liver disease (12, 14), raising the possibility that hepatic NIK might impair liver regeneration in these disease conditions. To model chronic liver disease, we treated NIK$^{\Delta hep}$ and NIK$^{f/f}$ male mice with 2-acetylaminofluorene (AAF), a hepatotoxin (25), for 10 days prior to PHx. Liver cell proliferation was assessed at 48 h post-PHx. AAF treatment considerably increased hepatic levels of NF-kB2 p52 in wild type mice, indicative of NIK activation (Figure 6A). Baseline

levels of proliferating $Ki67^+$ hepatocytes in resected livers (<2%) were comparable between $NIK^{f/f}$ and $NIK^{\Delta hep}$ mice (Figure 6B). PHx markedly increased hepatocyte proliferation rates in $NIK^{f/f}$ mice, which was substantially inhibited by AAF pretreatment (Figure 6C,D). Remarkably, the number of $Ki67^+$ hepatocytes was significantly higher in $NIK^{\Delta hep}$ relative to $NIK^{f/f}$ littermates following AAF and PHx treatments (Figure 6C,D). Liver to body weigh ratios were slightly higher in $NIK^{\Delta hep}$ relative to $NIK^{f/f}$ mice at 2 days post-PHx, but not statistically different (Figure 6-figure supplement 1A). As discussed above, a 2-day period may be too short for newly-generated hepatocytes to grow in size to significantly increase liver weight. Plasma ALT levels were also similar between $NIK^{f/f}$ and $NIK^{\Delta hep}$ mice (Figure 6E).

We next examined cell signaling that drives cell cycle progression. We detected baseline levels of phosphorylation of hepatic STAT3 in $NIK^{\Delta hep}$ but not $NIK^{f/f}$ mice after AAF pretreatment (Figure 6F). PHx stimulated STAT3 phosphorylation in both $NIK^{\Delta hep}$ and $NIK^{f/f}$ mice, but to a substantially higher level in $NIK^{\Delta hep}$ mice (Figure 6F). Baseline hepatic cyclin D1 levels were undetectable in both $NIK^{\Delta hep}$ and $NIK^{f/f}$ mice pretreated with AAF, and PHx increased cyclin D1 levels to a higher extent in $NIK^{\Delta hep}$ than in $NIK^{f/f}$ mice (Figure 6F). Together, these data support the notion that abnormal activation of hepatic NIK contributes to hepatotoxin-induced impairment in liver regeneration.

Inactivation of hepatic NIK increases reparative hepatocyte proliferation in mice with NAFLD. NAFLD is associated with both arrest of hepatocyte proliferation and upregulation of hepatic NIK (4, 5, 12, 14, 26), prompting us to test if elevated hepatic NIK is responsible for impairment in liver regeneration under the disease conditions. To model NAFLD, we placed $NIK^{\Delta hep}$ and $NIK^{f/f}$ mice on a high fat diet (HFD) for 10 weeks. Both $NIK^{\Delta hep}$ and $NIK^{f/f}$ mice similarly developed liver steatosis, as assessed by liver triacylglycerol (TAG) levels

(Figure 7A). HFD feeding increased hepatic NF-kB2 p52 levels, indicative of NIK activation (Figure 7B). To assess liver regeneration, we performed PHx after HFD feeding for 10 weeks. Hepatocyte proliferation was assessed at 48 h post-PHx by staining liver sections with anti-Ki67 antibody (Figure 7C). Baseline levels of hepatocyte proliferation in resected livers were comparable between $NIK^{\Delta hep}$ and $NIK^{f/f}$ mice (Figure 7D). PHx markedly increased hepatocyte proliferation in chow-fed $NIK^{f/f}$ mice, which was substantially inhibited by HFD feeding (Figure 7E). Importantly, number of proliferating $Ki67^{+}$ hepatocytes was significantly higher in $NIK^{\Delta hep}$ than in $NIK^{f/f}$ littermates after HFD feeding (Figure 7E). Liver/body weight ratios were slightly higher in $NIK^{\Delta hep}$ relative to $NIK^{f/f}$ mice at 2 days post-PHx, but not statistically different (Figure 6-figure supplement 1B). This modest difference can be explained by the short duration that limits the capacity of newly-generated hepatocytes to significantly grow in size and increase liver weight. Plasma ALT levels were comparable between $NIK^{\Delta hep}$ and $NIK^{f/f}$ littermates under both basal and PHx conditions (Figure 7F).

We further explored liver mitogenic pathways in these mice. Baseline STAT3 phosphorylation levels in resected livers were similar between $NIK^{\Delta hep}$ and $NIK^{f/f}$ mice fed a HFD; however, liver STAT3 phosphorylation increased to a considerably higher level in $NIK^{\Delta hep}$ relative to $NIK^{f/f}$ mice at 48 h post-PHx (Figure 7G). Hepatic cyclin D1 levels were also higher in $NIK^{\Delta hep}$ than in $NIK^{f/f}$ mice post-PHx (Figure 7G). These data suggest that aberrant activation of hepatic NIK suppresses hepatocyte proliferation and liver regeneration in NAFLD at least in part by inhibiting the JAK2/STAT3 pathway.

Discussion

Reparative hepatocyte proliferation plays a pivotal role in the maintenance of liver homeostasis and integrity by supplying new hepatocytes to replace lost hepatocytes. Liver

241 regeneration impairment is likely involved in chronic liver diseases. In this work, we identified
242 hepatic NIK and IKKα as unrecognized suppressors of liver regeneration; moreover, NIK
243 inhibits hepatocyte proliferation at least in part by activating IKKα. We previously demonstrated
244 that hepatic NIK is aberrantly activated in mice and humans with chronic liver disease (12, 14).
245 Our current results show that elevated activation of hepatic NIK pathways impairs liver
246 regeneration, likely contributing to liver disease progression.

247 We found that hepatocyte-specific ablation of NIK or IKKα substantially increases
248 hepatocyte proliferation in $NIK^{\Delta hep}$ or $IKK\alpha^{\Delta hep}$ mice following PHx. Accordingly, liver
249 regeneration rates were higher both in $NIK^{\Delta hep}$ relative to $NIK^{f/f}$ littermates and in $IKK\alpha^{\Delta hep}$
250 relative to $IKK\alpha^{f/f}$ mice. We observed that both NIK and IKKα bound to JAK2 and substantially
251 inhibited the ability of JAK2 to phosphorylate STAT3. Consistently, hepatocyte-specific ablation
252 of either NIK or IKKα substantially increased phosphorylation of hepatic JAK2 and STAT3 in
253 mice with PHx. IKKα deficiency decreased the ability of NIK to suppress the JAK2/STAT3
254 pathway in hepatocytes, confirming that IKKα acts downstream of NIK. However, NIK
255 overexpression still inhibited the JAK2/STAT3 pathway in IKKα-deficient hepatocytes,
256 suggesting that hepatic NIK is able to suppress the JAK2/STAT3 pathway by an additional
257 IKKα-independent mechanism. The JAK2/STAT3 pathway is known to drive hepatocyte
258 proliferation, which is indispensable for liver regeneration (19, 20, 22, 23). Therefore, hepatic
259 NIK and IKKα inhibit liver regeneration at least in part by suppressing the JAK2/STAT3
260 pathway.

261 Mounting evidence shows that hepatic NIK is aberrantly activated in chronic liver
262 disease, likely due to liver inflammation and hepatocellular stress (12, 14). We modeled chronic
263 liver disease by chronically treating mice with hepatotoxin AAF or placing them on HFD. We

found that hepatocyte-specific inactivation of NIK substantially increases the ability of PHx to stimulate hepatocyte proliferation in both AAF-treated mice and HFD-fed $NIK^{\Delta hep}$ mice. Consistently, in mice pretreated with AAF or HFD, ablation of hepatic NIK increased phosphorylation of both hepatic JAK2 and STAT3 post-PHx. It is worth mentioning that NIK in nonparenchymal cells (e.g. immune cells) also contributes to obesity-associated liver steatosis (27). These observations raise the possibility that in chronic liver disease, NIK in Kupffer cells/macrophages, and possibly other nonparenchymal cells, may indirectly inhibit reparative hepatocyte replication by a paracrine mechanism. Collectively, our results provide proof of concept evidence supporting the notion that aberrant hepatic NIK impairs reparative hepatocyte replication, thereby contributing to liver disease progression.

In conclusion, we have identified hepatic NIK and IKKα as unrecognized suppressors of reparative hepatocyte replication. NIK and IKKα suppress liver regeneration at least in part by inhibiting the hepatic JAK2/STAT3 pathway. Our findings suggest that pharmacological inhibition of hepatic NIK or IKKα may provide a new therapeutic strategy for liver disease treatment.

Materials and methods

Key Resources Table				
Reagent type	**Designation**	**Source or reference**	**Identifiers**	**Additional information**
Antibody	Ki67	Vector lab	VP-RM04	1:100
Antibody	NIK	Abcam	ab191591	1:2000
Antibody	IKK beta	Cell Signaling Technology	8943	1:5000

Antibody	IKK alpha	Cell Signaling Technology	2682	1:5000
Antibody	p-IKKa/b	Cell Signaling Technology	2697	1:5000
Antibody	STAT3	Santa Cruz	sc-8019	1:1000
Antibody	p-STAT3	Cell Signaling Technology	9145	1:5000
Antibody	JAK2	Cell Signaling Technology	3230	1:5000
Antibody	p-JAK2 1007/1008	Cell Signaling Technology	3776	1:5000
Antibody	Myc	Santa Cruz	sc-40	1:1000
Antibody	Flag	Sigma	F1804	1:5000
Antibody	p85	Home-raised	N/A	1:5000
Antibody	α-tubulin	Santa Cruz	sc-5286	1:1000
Antibody	JNK	Cell Signaling Technology	9258	1:5000
Antibody	p-JNK	Cell Signaling Technology	4668	1:5000
Antibody	ERK1/2	Cell Signaling Technology	9102	1:5000
Antibody	p-ERK1/2	Cell Signaling Technology	4370	1:5000
Antibody	NF-kB2	Cell Signaling Technology	4882	1:5000
Antibody	p65	Cell Signaling Technology	8242	1:5000
Antibody	p-p65	Cell Signaling Technology	3033	1:5000
Antibody	IkB alpha	Cell Signaling Technology	4812	1:5000
Antibody	p-IkB alpha	Cell Signaling Technology	9246	1:5000
Antibody	AKT	Cell Signaling Technology	4091	1:5000
Antibody	p-Akt	Cell Signaling Technology	4060	1:5000
Antibody	Cyclin D1	Cell Signaling Technology	2978	1:5000

Antibody	F4/80	eBioscience	14-4801	1:100
Antibody	HNF4 alpha	Santa Cruz	sc-8987	1:100
Antibody	CK8	Developmental Studies Hybridoma Bank	Troma I	1:100
Antibody	BrDU	Cell Signaling Technology	5292	1:100

Antibodies and Animals. Antibodies were described in the key resources table. Animal experiments were conducted following the protocols approved by the University of Michigan Institutional Animal Care and Use Committee (IACUC). We generated $NIK^{f/f}$, $NIK^{\Delta hep}$, and $IKK\alpha^{\Delta hep}$ mice (C57BL/6 background). $IKK\alpha^{f/f}$ mice (C57BL/6 background) were provided by Dr. Yinling Hu (the Inflammation and Tumorigenesis Section, National Cancer Institute). *Albumin-Cre* mice (C57BL/6 background) were from the Jackson laboratory (Bar Harbor, ME). Mice were housed on a 12-h light-dark cycle and fed a normal chow diet (9% fat; Lab Diet, St. Louis, MO) or a HFD (60% fat in calories; D12492, Research Diets, New Brunswick, NJ) *ad libitum* with free access to water.

PHx models. We followed published 2/3 PHx protocols (15). Briefly, $NIK^{f/f}$, $NIK^{\Delta hep}$, $IKK\alpha^{f/f}$, and $IKK\alpha^{\Delta hep}$ male mice (8-10 wks,) were anesthetized with isoflurane, followed by a ventral midline incision. The median and left lateral lobes (70% of the liver) were resected by pedicle ligations. Mice were euthanized after PHx, and tissues were harvested for histological and biochemical analyses. Mice were intraperitoneally injected, 12 h before euthanization, with BrdU (40 mg/kg body weight, ip) to label proliferating cells. A separate cohort was fed a HFD for 10 weeks prior to PHx. An additional cohort was treated with hepatotoxin 2-acetylaminofluorene (AAF) (10 mg/kg body weight, gavage) daily for 10 days prior to PHx.

Immunostaining. Liver frozen sections were prepared using a Leica cryostat (Leica Biosystems Nussloch GmbH, Nussloch, Germany), fixed in 4% paraformaldehyde for 30 min, blocked for 3 h with 5% normal goat serum (Life Technologies) supplemented with 1% BSA, and incubated with the indicated antibodies at 4^0C overnight. The sections were incubated with Cy2 or Cy3-conjugated secondary antibodies.

Cell cultures, transient transfection, and adenoviral transductions. Primary hepatocytes were prepared from mouse liver using type II collagenase (Worthington Biochem, Lakewood, NJ) and grown on William's medium E (Sigma) supplemented with 2% FBS, 100 units ml^{-1} penicillin, and 100 μg ml^{-1} streptomycin, and infected with adenoviruses as described previously (28). HEK293 cells were grown at 37°C in 5% CO_2 in DMEM supplemented with 25 mM glucose, 100 U ml^{-1} penicillin, 100 μg ml^{-1} streptomycin, and 8% calf serum. For transient transfection, cells were split 16-20 h before transfection. Expression plasmids were mixed with polyethylenimine (Sigma, St. Louis, MO) and introduced into cells. The total amount of plasmids was maintained constant by adding empty vectors. Cells were harvested 48 h after transfection for biochemical analyses.

Immunoprecipitation and immunoblotting. Cells or tissues were homogenized in a L-RIPA lysis buffer (50 mM Tris, pH 7.5, 1% Nonidet P-40, 150 mM NaCl, 2 mM EGTA, 1 mM Na_3VO_4, 100 mM NaF, 10 mM $Na_4P_2O_7$, 1 mM benzamidine, 10 μg ml^{-1} aprotinin, 10 μg ml^{-1} leupeptin, 1 mM phenylmethylsulfonyl fluoride). Tissue samples were homogenized in lysis buffer (50 mM Tris, pH 7.5, 1% Nonidet P-40, 150 mM NaCl, 2 mM EGTA, 1 mM Na_3VO_4, 100 mM NaF, 10 mM $Na_4P_2O_7$, 1 mM benzamidine, 10 μg/ml aprotinin, 10 μg/ml leupeptin; 1 mM phenylmethylsulfonyl fluoride). Proteins were separated by SDS-PAGE and immunoblotted with the indicated antibodies.

Real-time quantitative PCR (qPCR) and ROS assays. Total RNAs were extracted using TRIzol reagents (Life technologies). Relative mRNA abundance of different genes was measured using SYBR Green PCR Master Mix (Life Technologies, 4367659). Liver lysates were mixed with a dichlorofluorescein diacetate fluorescent (DCF, Sigma, D6883) probe (5 μM) for 1 h at 37^0C. DCF fluorescence was measured using a BioTek Synergy 2 Multi-Mode Microplate Reader (485 nm excitation and 527 nm emission).

Statistical Analysis. Data were presented as means ± sem. Differences between two groups was analyzed using two-tailed Student's t tests. $P < 0.05$ was considered statistically significant.

Acknowledgements

We thank Drs. Lin Jiang, Liang Sheng, Chengxin Sun, and Lei Yin and Michelle Jin for assistance and discussion. We thank Dr. Yinling Hu (Inflammation and Tumorigenesis Section, National Cancer Institute) for providing us with $IKK\alpha^{f/f}$ mice. This study was supported by grants DK091591, DK115646, DK114220 (to LR) and DK47918 (to MBO) from the National Institutes of Health (NIH), fellowship #2013/07313-4 from São Paulo Research Foundation (FAPESP) (AST), and grant 81420108006 (to YL) from National Natural Science Foundation of China. This work utilized the cores supported by the Michigan Diabetes Research and Training Center (NIH DK20572), the University of Michigan's Cancer Center (NIH CA46592), the University of Michigan Nathan Shock Center (NIH P30AG013283), and the University of Michigan Gut Peptide Research Center (NIH DK34933).

References

1. Rui L (2014) Energy metabolism in the liver. *Compr Physiol* 4(1):177-197.
2. Michalopoulos GK (2017) Hepatostat: Liver regeneration and normal liver tissue maintenance. *Hepatology* 65(4):1384-1392.
3. Miyaoka Y*, et al.* (2012) Hypertrophy and unconventional cell division of hepatocytes underlie liver regeneration. *Curr Biol* 22(13):1166-1175.
4. Richardson MM*, et al.* (2007) Progressive fibrosis in nonalcoholic steatohepatitis: association with altered regeneration and a ductular reaction. *Gastroenterology* 133(1):80-90.
5. Inaba Y*, et al.* (2015) Growth arrest and DNA damage-inducible 34 regulates liver regeneration in hepatic steatosis in mice. *Hepatology* 61(4):1343-1356.
6. Sancho-Bru P*, et al.* (2012) Liver progenitor cell markers correlate with liver damage and predict short-term mortality in patients with alcoholic hepatitis. *Hepatology* 55(6):1931-1941.
7. Michalopoulos GK (2013) Principles of liver regeneration and growth homeostasis. *Compr Physiol* 3(1):485-513.
8. Sato Y, Tsukada K, Matsumoto Y, & Abo T (1993) Interferon-gamma inhibits liver regeneration by stimulating major histocompatibility complex class II antigen expression by regenerating liver. *Hepatology* 18(2):340-346.
9. Wu X*, et al.* (2015) Oral ampicillin inhibits liver regeneration by breaking hepatic innate immune tolerance normally maintained by gut commensal bacteria. *Hepatology* 62(1):253-264.
10. Sun SC (2012) The noncanonical NF-kappaB pathway. *Immunol Rev* 246(1):125-140.
11. Xiao G, Harhaj EW, & Sun SC (2001) NF-kappaB-inducing kinase regulates the processing of NF-kappaB2 p100. *Mol Cell* 7(2):401-409.
12. Sheng L*, et al.* (2012) NF-kappaB-inducing kinase (NIK) promotes hyperglycemia and glucose intolerance in obesity by augmenting glucagon action. *Nat Med* 18(6):943-949.
13. Jiang B*, et al.* (2015) Carboxyl Terminus of HSC70-interacting Protein (CHIP) Down-regulates NF-kappaB-inducing Kinase (NIK) and Suppresses NIK-induced Liver Injury. *The Journal of biological chemistry* 290(18):11704-11714.
14. Shen H*, et al.* (2014) Mouse hepatocyte overexpression of NF-kappaB-inducing kinase (NIK) triggers fatal macrophage-dependent liver injury and fibrosis. *Hepatology* 60(6):2065-2076.
15. Mitchell C & Willenbring H (2008) A reproducible and well-tolerated method for 2/3 partial hepatectomy in mice. *Nat Protoc* 3(7):1167-1170.
16. Shen H*, et al.* (2017) Thymic NF-kappaB-inducing Kinase (NIK) Regulates CD4+ T Cell-elicited Liver Injury and Fibrosis in Mice. *J Hepatol*.
17. Wuestefeld T*, et al.* (2013) A Direct In Vivo RNAi Screen Identifies MKK4 as a Key Regulator of Liver Regeneration. *Cell* 153(2):389-401.
18. Pauta M*, et al.* (2016) Akt-mediated foxo1 inhibition is required for liver regeneration. *Hepatology* 63(5):1660-1674.
19. Wang H, Lafdil F, Kong X, & Gao B (2011) Signal transducer and activator of transcription 3 in liver diseases: a novel therapeutic target. *Int J Biol Sci* 7(5):536-550.
20. Shi SY*, et al.* (2017) Janus kinase 2 (JAK2) Dissociates Hepatosteatosis from Hepatocellular Carcinoma in Mice. *The Journal of biological chemistry*.
21. Rui L & Carter-Su C (1999) Identification of SH2-bbeta as a potent cytoplasmic activator of the tyrosine kinase Janus kinase 2. *Proc Natl Acad Sci U S A* 96(13):7172-7177.
22. Riehle KJ*, et al.* (2008) Regulation of liver regeneration and hepatocarcinogenesis by suppressor of cytokine signaling 3. *J Exp Med* 205(1):91-103.
23. Cressman DE*, et al.* (1996) Liver failure and defective hepatocyte regeneration in interleukin-6-deficient mice. *Science* 274(5291):1379-1383.
24. Liu B*, et al.* (2008) IKKalpha is required to maintain skin homeostasis and prevent skin cancer. *Cancer Cell* 14(3):212-225.

25. Laishes BA & Rolfe PB (1981) Search for endogenous liver colony-forming units in F344 rats given a two-thirds hepatectomy during short-term feeding of 2-acetylaminofluorene. *Cancer Res* 41(5):1731-1741.
26. Collin de l'Hortet A*, et al.* (2014) GH Administration Rescues Fatty Liver Regeneration Impairment by Restoring GH/EGFR Pathway Deficiency. *Endocrinology* 155(7):2545-2554.
27. Liu Y*, et al.* (2017) Liver NF-kappaB-Inducing Kinase Promotes Liver Steatosis and Glucose Counterregulation in Male Mice With Obesity. *Endocrinology* 158(5):1207-1216.
28. Zhou Y, Jiang L, & Rui L (2009) Identification of MUP1 as a regulator for glucose and lipid metabolism in mice. *The Journal of biological chemistry* 284(17):11152-11159.

Figure legends

Figure 1. Hepatocyte-specific ablation of NIK accelerates reparative hepatocyte proliferation. $NIK^{f/f}$ (n=7) and $NIK^{\Delta hep}$ (n=7) male mice (8 weeks) were subjected to PHx, and livers were harvested 48 h or 96 h later. (**A**) Representative immunostaining of liver sections (48 h after PHx) with anti-Ki67. (**B**) $Ki67^+$ cells were counted and normalized to total $DAPI^+$ cells. (**C**) Representative immunostaining of liver sections (48 h after PHx) with anti-BrdU antibodies. (**D-E**) Representative images of liver sections (48 h after PHx) costained with anti-Ki67 and anti-HNF4α antibodies (**D**) or anti-Ki67 and anti-F4/80 antibodies (**E**). (**F**) $Ki67^+HNF4\alpha^+$ and $Ki67^+F4/80^+$ cells were counted and normalized to total $Ki67^+$ cells. (**G**) Liver cell death were assessed 48 h after PHx using TUNEL reagents. (**H**) Plasma ALT levels. (**I**) Liver to body weight ratios (n=8 per group). Data were statistically analyzed with two-tailed Student's t test, and presented as mean ± SEM. *$p<0.05$.

Figure 2. Hepatic NIK deficiency upregulates cyclin D1 without altering NF-kB1, Akt, and MAPK pathways in the liver. $NIK^{f/f}$ and $NIK^{\Delta hep}$ male mice (8 weeks) were subjected to PHx. (**A-B**) Liver extracts were immunoblotted with anti-cyclin D1 antibody (48 h after PHx). Cyclin D1 levels were quantified and normalized to α-tubulin levels ($NIK^{f/f}$: n=4, $NIK^{\Delta hep}$: n=4). (**C**) Liver extracts were immunoblotted with the indicated antibodies (4 h after PHx). (**D**) Liver ROS

levels 48 h after PHx (normalized to liver weight). $NIK^{f/f}$: n=5, $NIK^{\Delta hep}$: n=6. (**E**) Liver cytokine expression was measured by qPCR and normalized to 36B4 expression (48 h after PHx). $NIK^{f/f}$: n=5, $NIK^{\Delta hep}$: n=5. Data were statistically analyzed with two-tailed Student's t test, and presented as mean ± SEM. *p<0.05.

Figure 3. NIK inhibits the JAK2/STAT3 pathway. (**A**) Liver extracts were prepared from $NIK^{f/f}$ and $NIK^{\Delta hep}$ males 4 h after PHx and immunoblotted with anti-phospho-JAK2 and anti-phospho-STAT3 antibodies. Phosphorylation of JAK2 (pTyr1007/1008) and STAT3 (pTyr705) was normalized to total JAK2 and STAT3 levels, respectively. (**B**) STAT3 and JAK2 were coexpressed with or without NIK in HEK293 cells. Cell extracts were immunoblotted with the indicated antibodies. (**C**) NIK was coexpressed with JAK2 in HEK293 cells. Cell extracts were immunoprecipitated (IP) and immunoblotted with the indicated antibodies. (**D**) Mouse primary hepatocytes were transduced with NIK or β-gal adenoviral vectors and stimulated with IL6 (10 ng/ml). Cell extracts were immunoblotted with the indicated antibodies. Data were statistically analyzed with two-tailed Student's t test, and presented as mean ± SEM. *p<0.05.

Figure 4. Ablation of hepatocyte IKKα accelerates hepatocyte reparative proliferation. (**A**) Tissue extracts were immunoblotted with anti-IKKα or anti-α-tubulin antibodies. (**B-F**) $IKK\alpha^{f/f}$ (n=6) and $IKK\alpha^{\Delta hep}$ (n=6) male littermates were subjected to PHx, and livers were harvested 48 h later. (**B**) Liver sections were immunostained with anti-Ki67 antibody, and $Ki67^+$ cells were counted and normalized to total $DAPI^+$ cells. Day 0 and 1: n=4 per group; day 3: $IKK\alpha^{f/f}$: n=6, $IKK\alpha^{\Delta hep}$: n=8; day 5: $IKK\alpha^{f/f}$: n=9, $IKK\alpha^{\Delta hep}$: n=8; day 7: $IKK\alpha^{f/f}$: n=6, $IKK\alpha^{\Delta hep}$: n=5. (**C**) Representative images of liver sections costained with anti-Ki67 and anti-HNF4α antibodies. (**D**) Liver cyclin D1 was measured by immunoblotting (normalized to α-tubulin levels). (**E**) TUNEL-positive cells in liver sections. (**F**) Liver to body weight ratios. Day 0 and 1: n=4 per group; day

3: IKKα$^{f/f}$: n=6, IKKα$^{\Delta hep}$: n=8; day 5: IKKα$^{f/f}$: n=9, IKKα$^{\Delta hep}$: n=8; day 7: IKKα$^{f/f}$: n=6, IKKα$^{\Delta hep}$: n=5. Data were statistically analyzed with two-tailed Student's t test, and presented as mean ± SEM. *p<0.05.

Figure 5. IKKα inhibits the JAK2/STAT3 pathway. (**A-B**) Liver extracts were prepared 4 h after PHx and immunoblotted with anti-phospho-JAK2 and anti-phospho-STAT3 antibodies. Phosphorylation of JAK2 (pTyr1007/1008) and STAT3 (pTyr705) was normalized to total JAK2 and STAT3 levels, respectively. IKKα$^{f/f}$: n=6, IKKα$^{\Delta hep}$: n=6. (**C**) IKKα and JAK2 were coexpressed in HEK293 cells. Cell extracts were immunoprecipitated (IP) and immunoblotted with the indicated antibodies. (**D**) STAT3 and JAK2 were coexpressed with IKKα in HEK293 cells. Cell extracts were immunoblotted with the indicated antibodies. Data were statistically analyzed with two-tailed Student's t test, and presented as mean ± SEM. *p<0.05.

Figure 6. Ablation of hepatocyte NIK reverses AAF-induced impairment in hepatocyte reparative proliferation. (**A**) C57BL/6 males (8 weeks) were treated with PBS or AAF (10 mg/kg body weight, gavage) daily for 10 days. NF-kB2 p52 in liver extracts was immunoblotted with anti-NF-kB2 antibody (normalized to α-tubulin levels). PBS: n=4, AAF: n=4. (**B-G**) NIK$^{f/f}$ and NIK$^{\Delta hep}$ males were treated with PBS or AAF (10 mg/kg body weight) for 10 days and then subjected to PHx. Livers were harvested 48 h later. (**B**) Baseline Ki67^{+} cell number in resected liver sections obtained from PHx. NIK$^{f/f}$: n=5, NIK$^{\Delta hep}$: n=4. (**C**) Representative immunostaining of liver sections (AAF-treated) with anti-Ki67 antibody. (**D**) Ki67^{+} cell number in liver sections (normalized to DAPI^{+} cells). PBS;NIK$^{f/f}$: n=3, AAF;NIK$^{f/f}$: n=5, AAF;NIK$^{\Delta hep}$: n=5. (**E**) Plasma ALT levels. NIK$^{f/f}$: n=3, NIK$^{\Delta hep}$: n=4. (**F**) Liver extracts were immunoblotted with the indicated antibodies. Data were statistically analyzed with two-tailed Student's t test, and presented as mean ± SEM. *p<0.05.

Figure 7. Hepatic NIK deficiency corrects impaired hepatocyte reparative proliferation in mice with NAFLD. (**A-B**) C57BL/6 males (8 weeks) were fed a normal chow diet (n=5) or a HFD (n=5) for 10 weeks. (**A**) Liver TAG levels (normalized to liver weight). (**B**) NF-kB2 p52 in liver extracts was immunoblotted with anti-NF-kB2 antibody (normalized to α-tubulin levels). (**C-H**) $NIK^{f/f}$ and $NIK^{\Delta hep}$ males were fed a HFD for 10 weeks followed by PHx, and livers were harvested 48 h after PHx. (**C**) Representative immunostaining of liver sections with anti-Ki67 antibody. (**D**) Baseline $Ki67^{+}$ cell number in resected liver sections obtained from PHx. $NIK^{f/f}$: n=4, $NIK^{\Delta hep}$: n=4. (**E**) Liver $Ki67^{+}$ cell number (normalized to $DAPI^{+}$ cells). Chow;$NIK^{f/f}$: n=3, HFD;$NIK^{f/f}$: n=5, HFD; $NIK^{\Delta hep}$: n=4. (**F**) Plasma ALT levels. $NIK^{f/f}$: n=3, $NIK^{\Delta hep}$: n=4. (**G**) Liver extracts were immunoblotted with the indicated antibodies. Data were statistically analyzed with two-tailed Student's t test, and presented as mean ± SEM. *$p<0.05$.

Figure 2-figure supplement 1. Effect of PHx on liver NIK pathway activation. PHx was performed on C57BL/6 male mice. (**A**) Liver *NIK* mRNA abundance was measured by qPCR (normalized to 36B4 levels, n=3 per group). (**B-C**) Liver extracts were immunoblotted with antibodies against phospho-IKKα/β, IKKα and α-tubulin. Liver phospho-IKKα/β (normalized to IKKα levels) and IKKα (normalize to α-tubulin levels) levels were measured on days 0-7 following PHx. (**D**) PHx was performed on $NIK^{f/f}$ and $NIK^{\Delta hep}$ male mice. Liver extracts were prepared from resected livers and blotted with antibodies against phospho-STAT3, STAT3, phospho-JAK2, and JAK2. Data were statistically analyzed with two-tailed Student's t test, and presented as mean ± SEM. *$p<0.05$.

Figure 5-figure supplement 1. The effect of PHx on activation of liver IKKα and JAK2/STAT3 pathways. $IKK\alpha^{f/f}$ and $IKK\alpha^{\Delta hep}$ male mice were subjected to PHx, and livers were harvested on days 0-7. (**A**) Liver extracts were immunoblotted with the indicated

antibodies. (**B**) Phosphorylation of JAK2 (normalized to total JAK2 levels) and STAT3 (normalized to total STAT3) were analyzed using ANOVA (n=3 per group). IKKα phosphorylation (Figure 2-figure supplement 1C) was replotted here. (**C-D**) Primary hepatocytes were transduced with GFP or NIK adenoviral vectors and stimulated with IL6 (10 ng/ml) for 15 min. Cell extracts were immunoblotted with the indicated antibodies. Phosphorylation of STAT3 were normalized to total STAT3 (n=3 per group). Data were statistically analyzed with two-tailed Student's t test, and presented as mean ± SEM. *$p<0.05$.

Figure 6-figure supplement 1. Hepatic NIK inhibits reparative hepatocyte proliferation. (**A**) $NIK^{f/f}$ and $NIK^{\Delta hep}$ males were treated with PBS or AAF (10 mg/kg body weight) for 10 days and then subjected to PHx. Resected liver weight and liver weight 2 days post-PHx were normalized to body weight. Resected: n=3 per group; PHx: n=5 per group. (**B**) $NIK^{f/f}$ and $NIK^{\Delta hep}$ males were fed a HFD for 10 weeks followed by PHx. Resected liver weight and liver weight 2 days post-PHx were normalized to body weight. Resected: n=5 per group; PHx: n=5 per group. Data were statistically analyzed with two-tailed Student's t test, and presented as mean ± SEM.

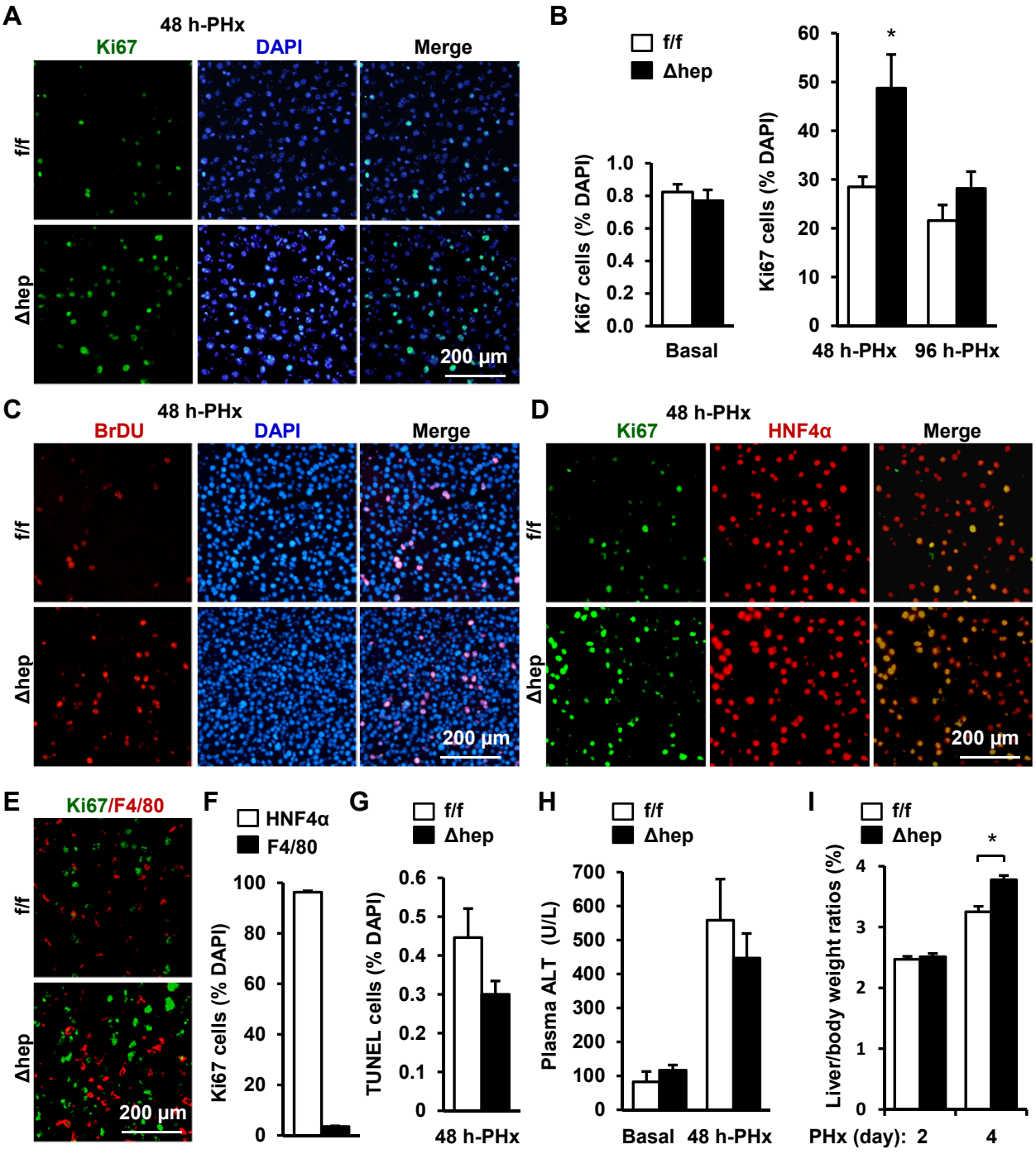
A
48 h-PHx
Ki67
DAPI
Merge
f/f
Δhep
200 μm
B
f/f
Δhep
Ki67 cells (% DAPI)
1.0
0.8
0.6
0.4
0.2
0.0
Basal
60
50
40
30
20
10
0
*
48 h-PHx
96 h-PHx
C
48 h-PHx
BrDU
DAPI
Merge
f/f
Δhep
200 μm
D
48 h-PHx
Ki67
HNF4α
Merge
f/f
Δhep
200 μm
E
Ki67/F4/80
f/f
Δhep
200 μm
F
HNF4α
F4/80
Ki67 cells (% DAPI)
100
80
60
40
20
0
G
f/f
Δhep
TUNEL cells (% DAPI)
0.6
0.5
0.4
0.3
0.2
0.1
0
48 h-PHx
H
f/f
Δhep
Plasma ALT (U/L)
700
600
500
400
300
200
100
0
Basal
48 h-PHx
I
f/f
Δhep
*
Liver/body weight ratios (%)
4
3
2
1
0
PHx (day): 2
4

Fig. 2

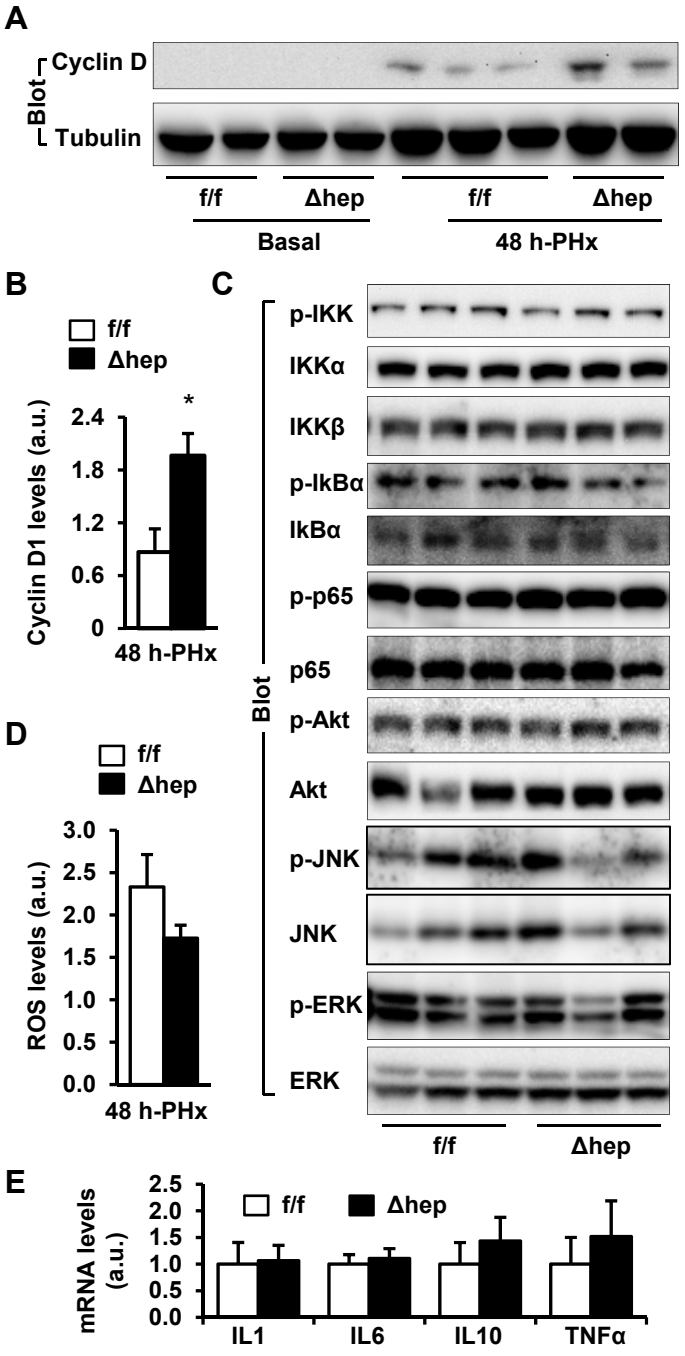
A
Blot
Cyclin D
Tubulin
f/f
Δhep
f/f
Δhep
Basal
48 h-PHx
B
f/f
Δhep
Cyclin D1 levels (a.u.)
2.4
1.8
1.2
0.6
0
*
48 h-PHx
C
Blot
p-IKK
IKKα
IKKβ
p-IkBα
IkBα
p-p65
p65
p-Akt
Akt
p-JNK
JNK
p-ERK
ERK
f/f
Δhep
D
f/f
Δhep
ROS levels (a.u.)
3.0
2.5
2.0
1.5
1.0
0.5
0.0
48 h-PHx
E
mRNA levels (a.u.)
2.5
2.0
1.5
1.0
0.5
0.0
f/f
Δhep
IL1
IL6
IL10
TNFα

Figure 2-figure supplement 1

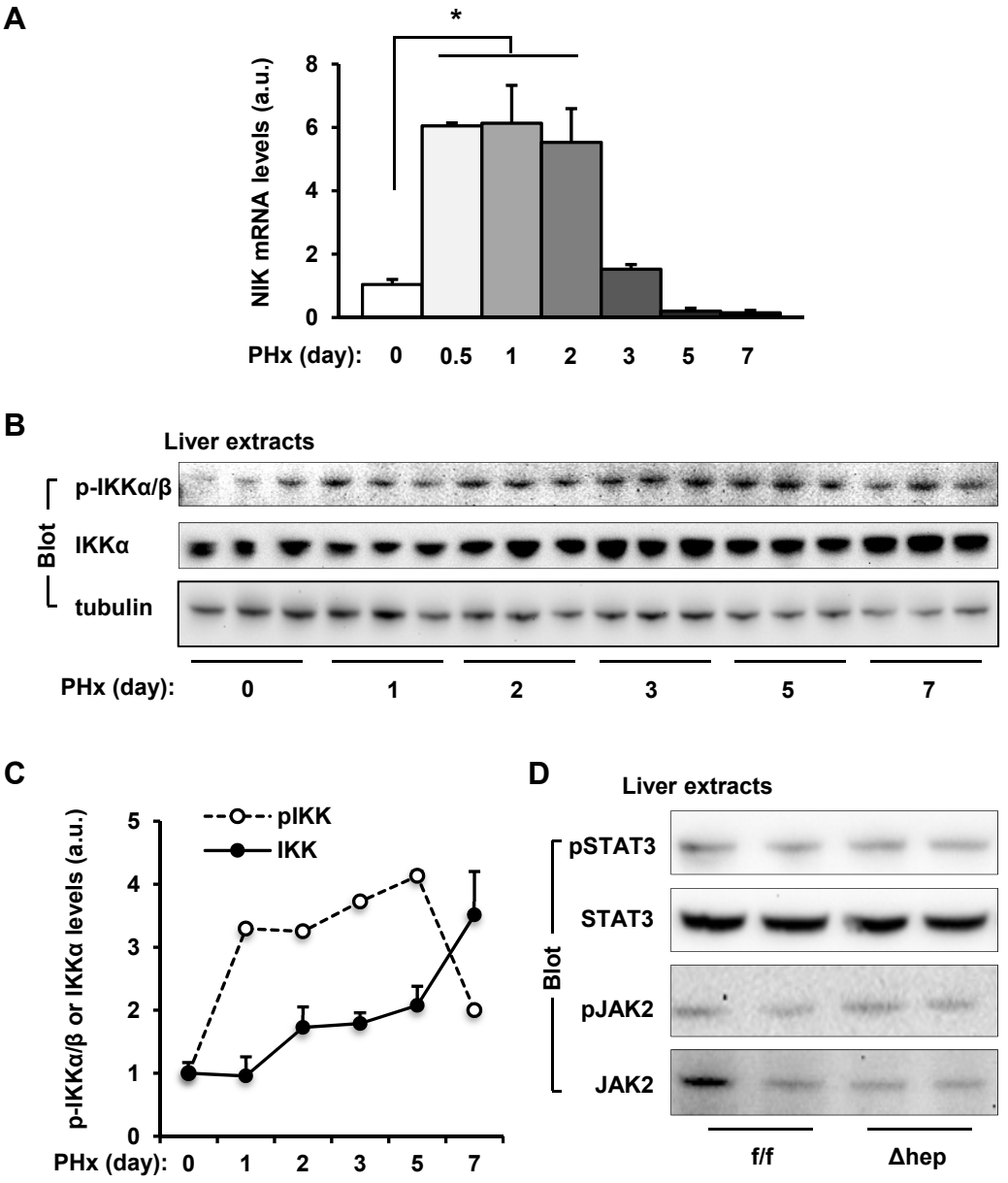

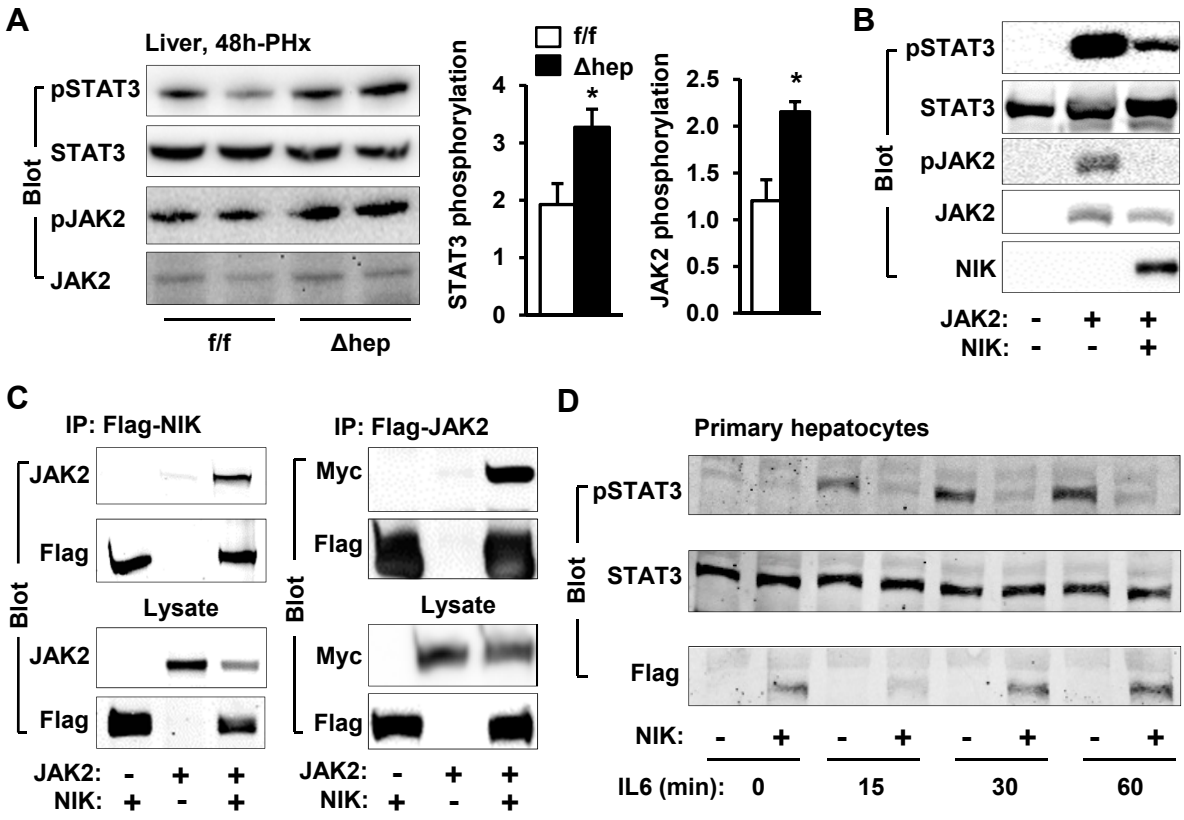
A
Liver, 48h-PHx
pSTAT3
STAT3
pJAK2
JAK2
Blot
f/f
Δhep
STAT3 phosphorylation
JAK2 phosphorylation
B
pSTAT3
STAT3
pJAK2
JAK2
NIK
Blot
JAK2:
NIK:
C
IP: Flag-NIK
IP: Flag-JAK2
JAK2
Flag
Myc
Lysate
Blot
D
Primary hepatocytes
pSTAT3
STAT3
Flag
Blot
NIK:
IL6 (min): 0 15 30 60

Fig. 4

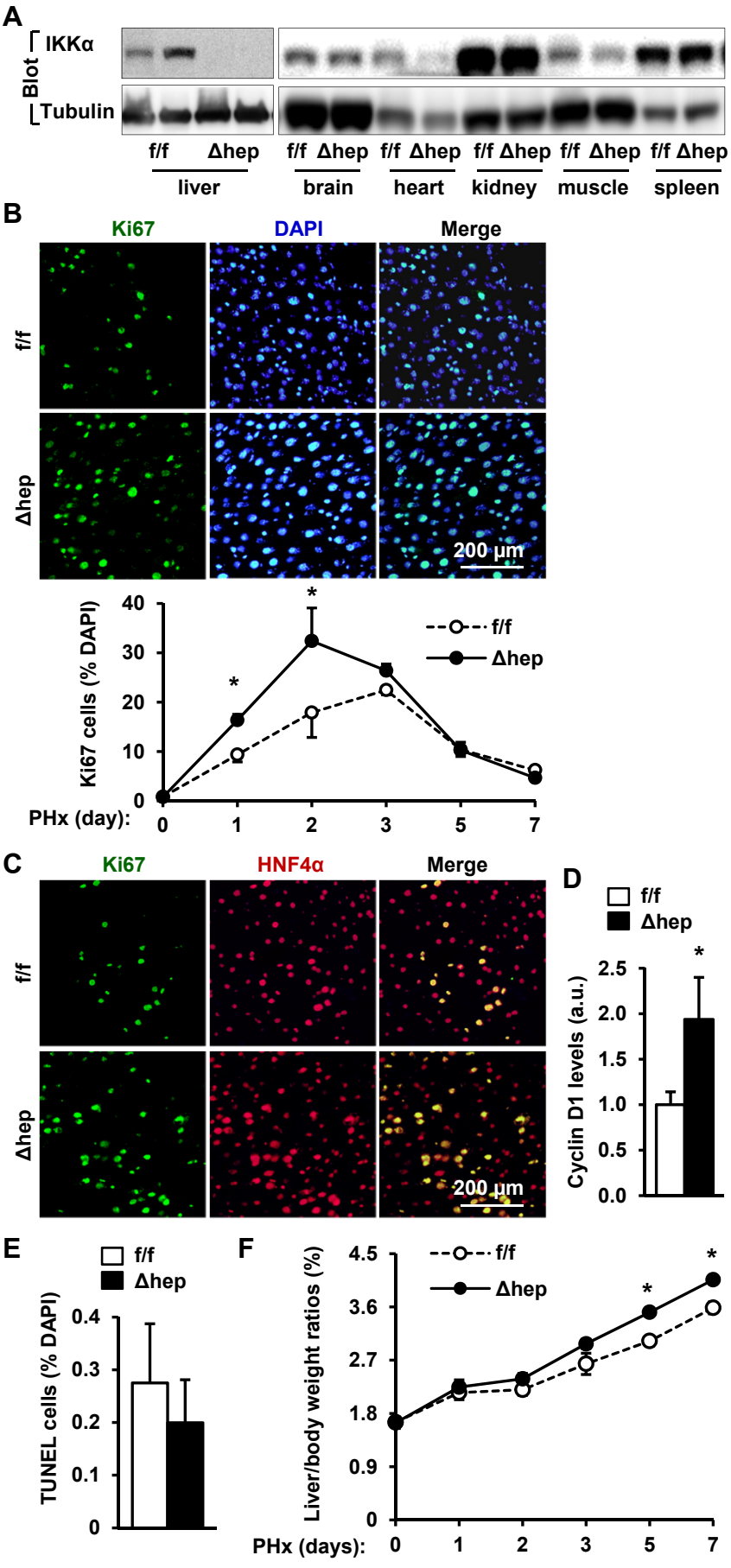
A
Blot
IKKα
Tubulin
f/f Δhep f/f Δhep f/f Δhep f/f Δhep f/f Δhep f/f Δhep
liver brain heart kidney muscle spleen
B
Ki67 DAPI Merge
f/f
Δhep
200 μm
Ki67 cells (% DAPI)
40 30 20 10 0
PHx (day): 0 1 2 3 5 7
f/f
Δhep
C
Ki67 HNF4α Merge
f/f
Δhep
200 μm
D
f/f
Δhep
Cyclin D1 levels (a.u.)
2.5 2.0 1.5 1.0 0.5 0.0
E
f/f
Δhep
TUNEL cells (% DAPI)
0.4 0.3 0.2 0.1 0
F
f/f
Δhep
Liver/body weight ratios (%)
4.5 3.6 2.7 1.8 0.9 0
PHx (days): 0 1 2 3 5 7

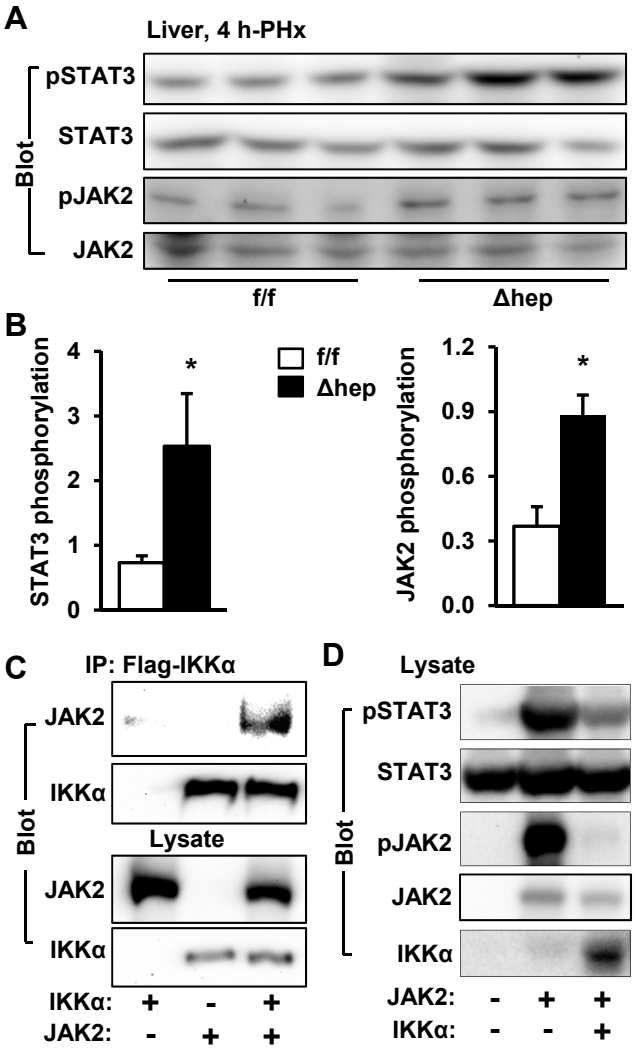
A
Liver, 4 h-PHx
pSTAT3
STAT3
pJAK2
JAK2
Blot
f/f
Δhep
B
STAT3 phosphorylation
JAK2 phosphorylation
f/f
Δhep
*
*
C
IP: Flag-IKKα
JAK2
IKKα
Lysate
JAK2
IKKα
Blot
IKKα: + - +
JAK2: - + +
D
Lysate
pSTAT3
STAT3
pJAK2
JAK2
IKKα
Blot
JAK2: - + +
IKKα: - - +

Figure 5-figure supplement 1

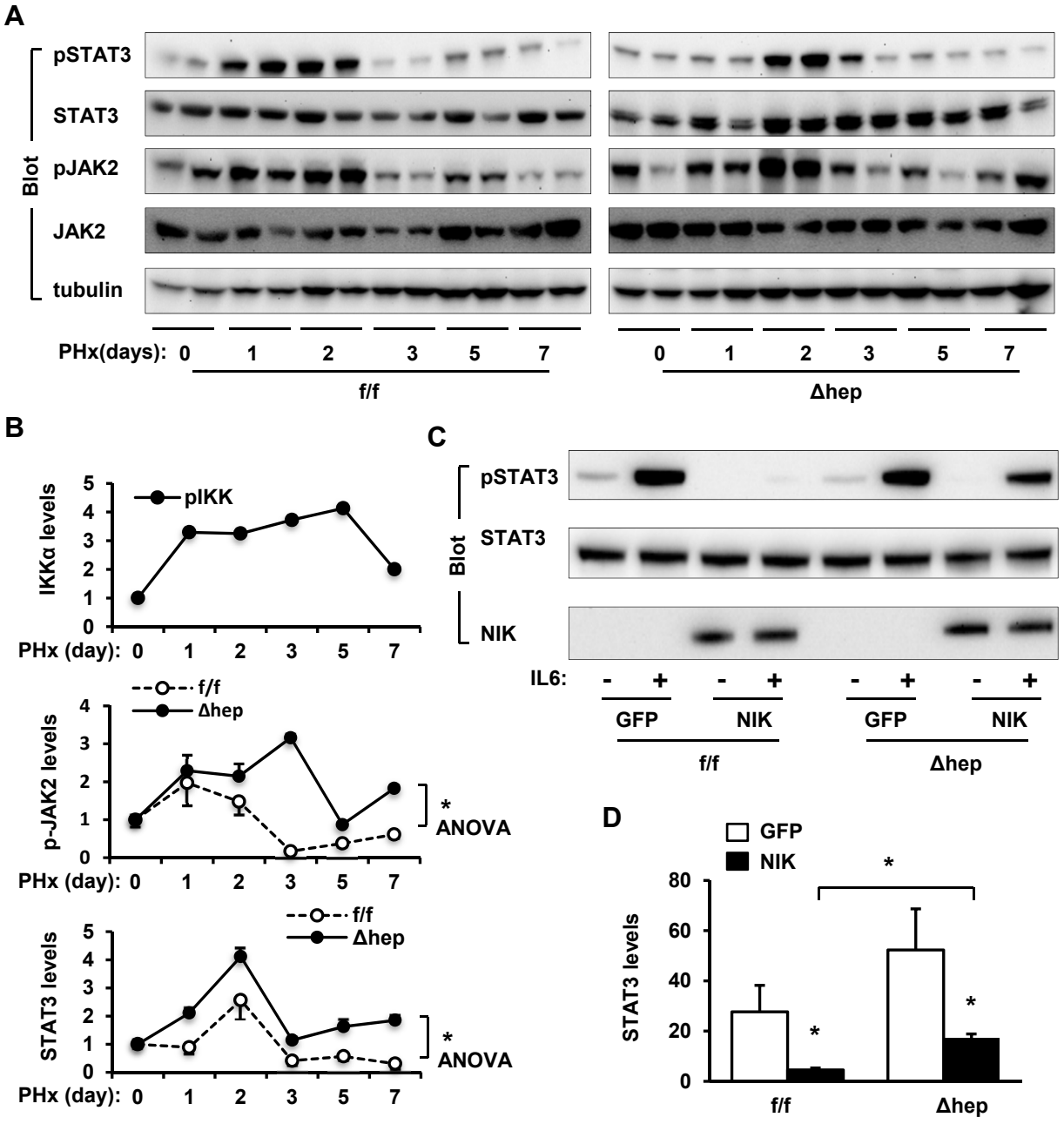

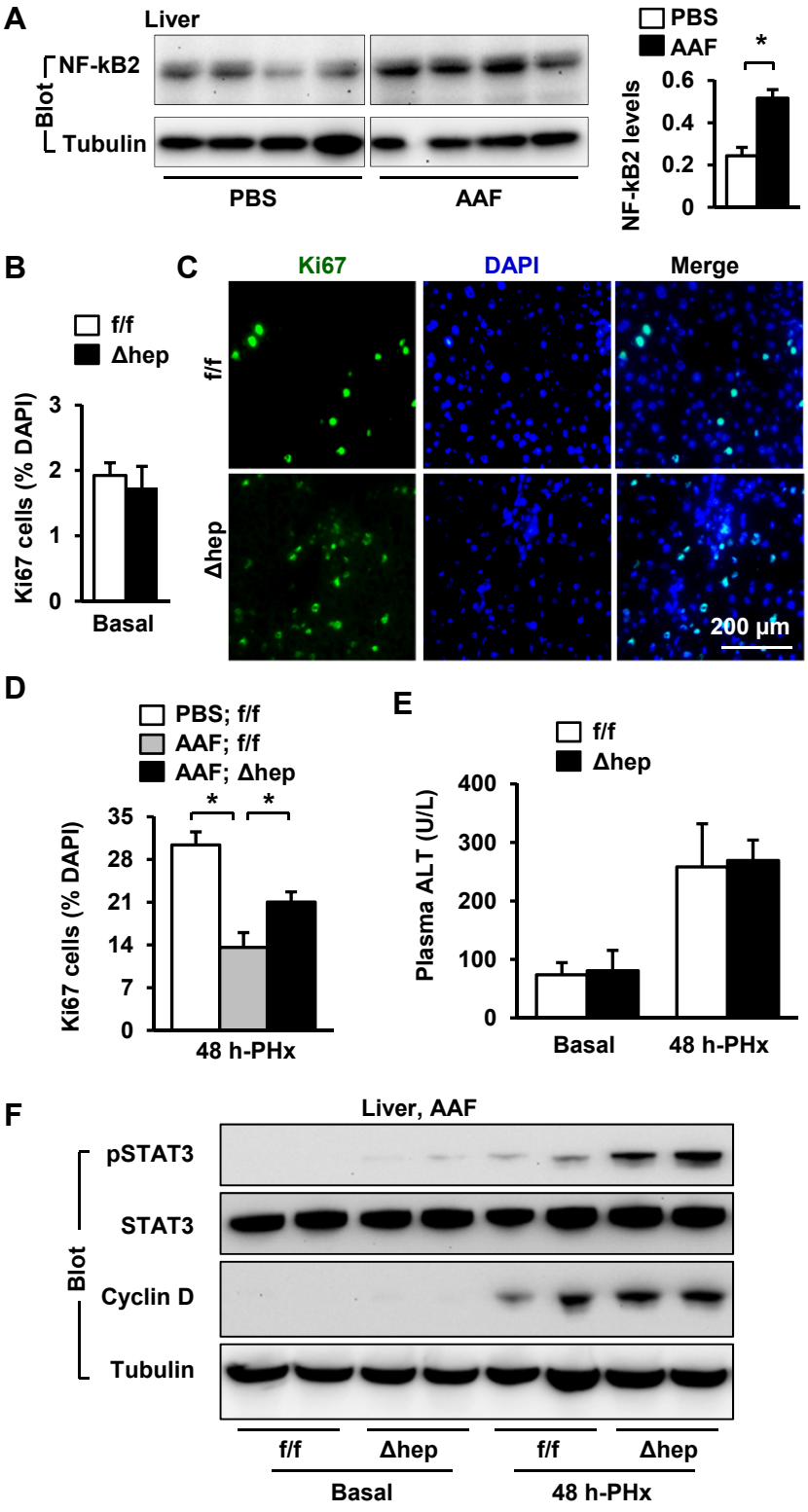
A
Liver
NF-kB2
Blot
Tubulin
PBS
AAF
PBS
AAF
*
NF-kB2 levels
0.6
0.4
0.2
0
B
f/f
Δhep
Ki67 cells (% DAPI)
3
2
1
0
Basal
C
Ki67
DAPI
Merge
f/f
Δhep
200 μm
D
PBS; f/f
AAF; f/f
AAF; Δhep
*
*
Ki67 cells (% DAPI)
35
28
21
14
7
0
48 h-PHx
E
f/f
Δhep
Plasma ALT (U/L)
400
300
200
100
0
Basal
48 h-PHx
F
Liver, AAF
pSTAT3
STAT3
Cyclin D
Tubulin
Blot
f/f
Δhep
f/f
Δhep
Basal
48 h-PHx

Figure 6-figure supplement 1

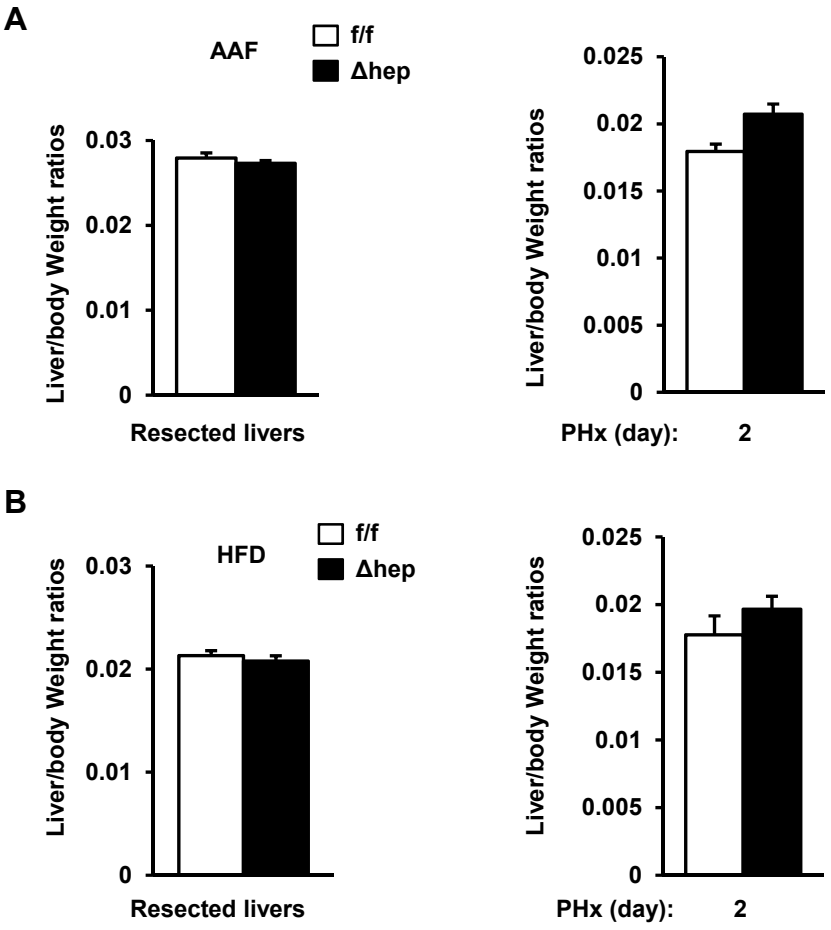

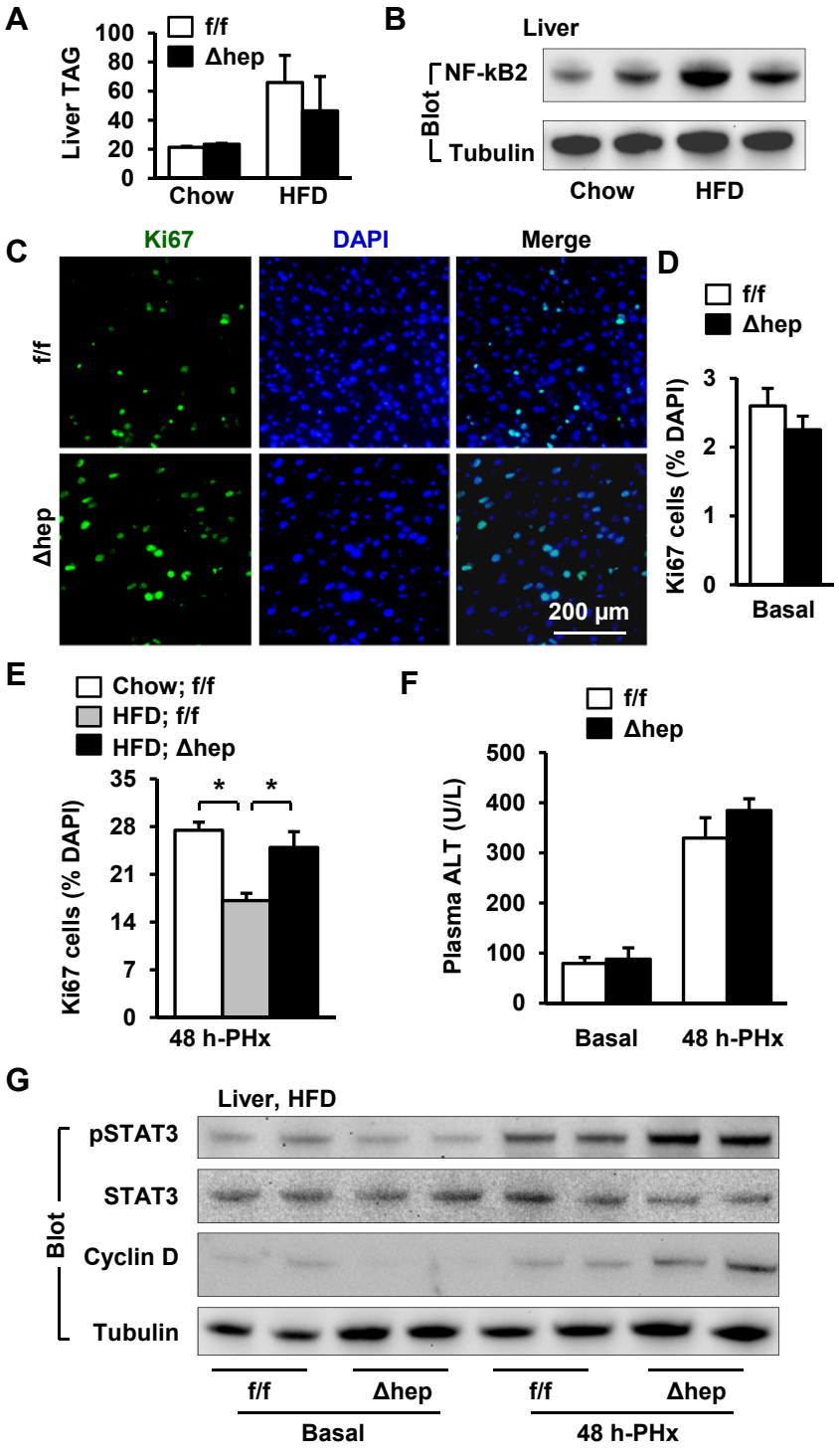
A
Liver TAG
100
80
60
40
20
0
f/f
Δhep
Chow
HFD
B
Liver
Blot
NF-kB2
Tubulin
Chow
HFD
C
Ki67
DAPI
Merge
f/f
Δhep
200 μm
D
f/f
Δhep
Ki67 cells (% DAPI)
3
2
1
0
Basal
E
Chow; f/f
HFD; f/f
HFD; Δhep
Ki67 cells (% DAPI)
35
28
21
14
7
0
*
*
48 h-PHx
F
f/f
Δhep
Plasma ALT (U/L)
500
400
300
200
100
0
Basal
48 h-PHx
G
Liver, HFD
Blot
pSTAT3
STAT3
Cyclin D
Tubulin
f/f
Δhep
f/f
Δhep
Basal
48 h-PHx